CHEMISTRY OF MATERIALS

Article

pubs.acs.org/cm

Tuning the Adsorption of Polysulfides in Lithium–Sulfur Batteries with Metal–Organic Frameworks

Haesun Park[†] and Donald J. Siegel*[,†,‡,§,∥,⊥]

[†]Mechanical Engineering Department, [‡]Materials Science & Engineering, [§]Applied Physics Program, [∥]Michigan Energy Institute, and [⊥]Joint Center for Energy Storage Research, University of Michigan, Ann Arbor, Michigan 48109-2125, United States

Supporting Information

ABSTRACT: The dissolution of polysulfide (PS) intermediates during discharge is a well-known obstacle to achieving long cycle life in lithium–sulfur batteries. Prior work has shown that PS dissolution can be partially suppressed via physical encapsulation of sulfur and PS within a porous cathode support. Metal–organic frameworks (MOFs) are crystalline, nanoporous materials with extremely high surface areas, whose structure and composition can be varied extensively. MOFs are promising cathode support materials because the encapsulation afforded by MOF pores can be augmented by chemical adsorption of PS onto coordinately unsaturated metal sites (CUS). Here, we demonstrate that this additive approach—restricting PS dissolution by combining encapsulation and adsorption within a MOF—can be tuned to maximize PS anchoring via metal substitution on the CUS. Optimal MOF compositions are pinpointed by computationally screening 16 metal-substituted variants of M_2(dobdc) (MOF-74) for their ability to chemically anchor prototypical species (S_8, Li_2S_4, and Li_2S) present during the cycling of Li–S batteries. Ti_2, Ni_2, and Mo_2(dobdc) are identified as the compositions with the largest affinities for Li_2S_4 and Li_2S. As Ni_2(dobdc) has been synthesized previously, this MOF is proposed as a promising cathode support for Li–S batteries.

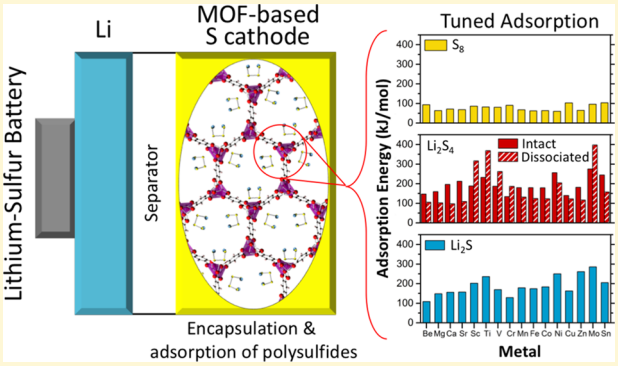

INTRODUCTION

The lithium–sulfur (Li–S) electrochemical couple has received significant attention as a potential next-generation battery chemistry due to its high theoretical energy density (2199 Wh/L and 2567 Wh/kg),[1,2] potential for low cost, and nontoxic manufacturing process.[3] Li–S cells discharge via the overall reaction $2Li + S \rightarrow Li_2S$ with an average potential of approximately 2.2 V. Despite these benefits, the commercial viability of Li–S batteries is presently limited by their tendency to undergo capacity fade upon cycling. This effect can be traced to the so-called "poly-sulfide shuttle,"[4] which arises from the formation of polysulfide (Li_2S_x) intermediates during discharge. The polysulfides (PS) are highly soluble in conventional organic liquid electrolytes. This solubility is deemed to be undesirable, as it can result in uncontrolled deposition of the Li_2S discharge product within the positive electrode, and crossover of PS to the anode. Both processes result in a loss of active material. For example, deposition of insulating Li_2S on the anode surface can impede charge transfer, limiting capacity and power density.[5,6] Self-discharge has also been attributed to the dissolution of PS.[7]

Given the performance limitations arising from polysulfide dissolution, many strategies have been proposed to confine the PS, or dramatically reduce their solubility.[8−21] Perhaps the most widely studied strategy employs physical encapsulation of sulfur and PS. For example, Nazar et al.[22] used mesoporous carbon to encapsulate elemental sulfur and the discharge products within the cathode. Approaches[22−27] involving infiltration of molten sulfur into hollow carbon materials also enhance the cyclability of Li–S cells. However, due to the weak interaction between PS and these host materials, the confinement is often imperfect, and some PS eventually escape.[28]

As an alternative strategy to physical encapsulation, Nazar and co-workers proposed that capacity retention can be strongly influenced by the surface area of the cathode support and the support's affinity for PS.[29] This was demonstrated by comparing the performance of supports based on porous carbons (Super P, Vulcan, FW200), Ti_4O_7-C, electrolytic manganese dioxide (EMD), anatase-TiO_2, meso-TiO_2, graphene oxide (GO), and MnO_2. Materials with strong PS adsorption exhibited low irreversible capacity loss. Improved cyclability attributed to PS adsorption has also been observed in cells where 2-D materials such as SiO_2[30] and TiO_2[31] were added to the cathode. Cui et al. designed yolk–shell structures using TiO_2[32] and various metal sulfides[33] that showed low capacity fade (0.033%/cycle). The bonding between 2-D metal chalcogenides and polysulfide species/S_8/Li_2S was examined computationally.[34] The use of metal chalcogenides as cathode

Received: March 22, 2017
Revised: May 4, 2017
Published: May 5, 2017

DOI: 10.1021/acs.chemmater.7b01166
Chem. Mater. XXXX, XXX, XXX–XXX

supports also showed improvement in performance.[35−39] Additional development of these strategies is needed to simultaneously achieve high sulfur loadings and PS retention.[28]

The foregoing discussion highlights encapsulation and adsorption as two strategies for limiting PS dissolution. At present, it appears that neither approach is sufficient on its own; therefore, it is natural to ask whether superior performance could be achieved through their *combination*. For this approach to succeed, a porous cathode support with a high density of adsorption sites is needed. Metal−organic frameworks (MOFs) are one class of materials that can satisfy these requirements. MOFs are microporous, crystalline materials made via self-assembly of metal clusters and organic linkers.[40] Due to their high surface areas, structural diversity, and potential to exhibit coordinately unsaturated metal sites (CUS), MOFs are candidates for use in a wide variety of applications, including the storage of molecular species such as CO_2,[40−42] CH_4,[43,44] and H_2.[45−47] An additional advantage of MOFs is that their composition—and, consequently, their performance—can be tuned via metal substitution.[40]

Among the thousands of reported MOFs, the compound M_2(dobdc)[48] exhibits several properties that are conducive to its use as a Li−S cathode support. [M_2(dobdc) is composed of unsaturated metal $(M)^{2+}$ ions in a square-pyramidal coordination arranged in linear, infinite chains linked by 2,5-dioxido-1,4-benzene dicarboxylate (dobdc) linkers.] First, the nanoscale pores of M_2(dobdc) are arranged in a 1-D close-packed (honeycomb) structure, consistent with low-tortuosity access of Li ions and encapsulation of active materials. Second, the density of CUS in M_2(dobdc) is the highest for any known MOF, thereby providing a high number of PS adsorption sites. Finally, the surface area of M_2(dobdc), > ∼1000 m^2/g,[49] is much higher than that of other sulfur host materials (< ∼300 m^2/g),[29] consistent with a high sulfur loading.

On the basis of these data, and following the analysis performed in ref 29, the adsorption capacity of M_2(dobdc) is predicted to range from 6.6 to 13.4 mg of Li_2S_4 per 10 mg of MOF. (The capacity range arises from variations in the CUS composition; we also assume 1 molecule of Li_2S_4 is adsorbed per CUS.) These theoretical capacities outperform the best sulfur support material demonstrated in the literature, MnO_2, which has an adsorption capacity of ∼6 mg of Li_2S_4/10 mg of MnO_2.[29] Other examples include TiO_2 (∼2.5 mg/10 mg) and graphene oxide (∼5 mg/10 mg).[29]

Despite these potential benefits, studies exploring the use of MOFs in Li−S battery cathodes are relatively rare.[28] To our knowledge, the earliest study to employ MOFs in these batteries was that of Tarascon et al., who reported the performance of a MIL-100(Cr)-based composite cathode.[50] Subsequently, Zhou et al. examined ZIF-8, MIL-53(Al), NH_2-MIL-53(Al), and HKUST-1-based cathodes and demonstrated that a ZIF-8-based electrode can achieve 300 cycles at relatively high rates (0.5 C), corresponding to a capacity fade of only 0.08%/cycle.[51] Qian et al. demonstrated an HKUST-1-based cathode with a high sulfur loading (40 wt % of the S+MOF mass), a lifetime of 170 cycles, and a capacity at the conclusion of cycling of approximately 500 mAh/g.[52] Wang et al. explored composite cathodes based on the MOF-525 series.[53] A cell using MOF-525(Cu) demonstrated the best performance to-date for a S/MOF composite cathode, with a reversible capacity of 700 mAh/g after 200 cycles at 0.5 C.[53] Zheng et al. examined Ni- and Co-MOF-based S cathodes experimentally and computationally.[54] The Ni-MOF cathode exhibited superior performance (89% capacity retention over 100 cycles at 0.1 C), which was attributed to the synergistic effects of physical encapsulation and strong interactions between PS and the Ni(II) sites. Finally, MOFs have also been examined as solid electrolyte hosts in Li-ion batteries[55] and as separators in Li−S batteries.[56]

The goal of the present study is to identify MOFs that maximize Li_xS_y adsorption by combining physical encapsulation within the MOF pores with strong chemical anchoring to the MOF. Ideally, such a MOF support would constrain both redox end members (S and Li_2S) and all PS intermediates present during operation of a Li−S cell. In this case, there is no need for any S-containing species to migrate into or out of the MOF pores, assuming these species remain accessible to Li^+ and electrons. Given its high density of adsorption sites and 1-D porosity, we adopt M_2(dobdc) as a prototype MOF and investigate computationally how metal substitution on the CUS impacts the adsorption of PS. More specifically, first-principles calculations are used to screen 16 metal-substituted variants of M_2(dobdc) (M = Be, Mg, Ca, Sr, Sc, Ti, V, Cr, Mn, Fe, Co, Ni, Cu, Zn, Mo, Sn) with respect to their adsorption energies for prototypical species present during the cycling of Li−S batteries: S_8, Li_2S_4, and Li_2S.

Our calculations reveal that the CUS is the dominant adsorption site for all species examined. Nevertheless, significant differences exist in the strength and nature of the adsorption across the three adsorbates. Adsorption of S_8 is generally weakest, and relatively insensitive to the composition of the CUS. On the other hand, adsorption of Li_2S_4 and Li_2S is typically much stronger, approaching ∼400 kJ/mol, and is highly sensitive to CUS composition. A tendency for spontaneous decomposition of the Li_2S_4 molecule is observed for some CUS compositions, yielding very strong adsorption. Trends in the electronic structure for the different systems are examined in terms of Bader charges and spatial charge density differences.

Out of the 16 M_2(dobdc) compositions examined, compounds with M = Ti, Ni, and Mo were identified as having the largest affinities for Li_2S_4 and Li_2S. As the Ni-based variant has been synthesized previously, this MOF is proposed as a promising cathode support for Li−S batteries. An additional benefit of the "encapsulation plus adsorption" strategy is its ability to be combined with electrolyte-based tactics for minimizing PS dissolution, such as the use of electrolytes that are nonsolvating for PS.[57−59]

METHODS

Density Functional Theory (DFT)[60] calculations were performed using the Vienna Ab initio Simulation Package (VASP).[61,62] Long-range dispersion interactions between polysulfides and the MOF support were accounted for using a van der Waals-aware density functional (vdW-DF2).[63,64] In cases where the MOF CUS contained a transition metal, a Hubbard U correction[65] was also applied to describe the localization of d-electrons more accurately.[66] The plane-wave cutoff energy was set to 500 eV, and k-point sampling was performed at the Γ-point. All calculations were spin-polarized.

Metal-substituted dobdc crystal structures were adopted from our prior studies.[40] The internal degrees of freedom for these structures were relaxed to a force tolerance of 0.01 eV/Å using the vdW-DF2(+U) functional. Similarly, the adsorbate molecules (S_8, Li_2S_4, and Li_2S) were relaxed to a force tolerance of 0.01 eV/Å using the vdW-DF2 functional in a computational cell having the same shape and size as that for Ni_2(dobdc), but with the MOF atoms absent.

DOI: 10.1021/acs.chemmater.7b01166
Chem. Mater. XXXX, XXX, XXX−XXX

Low energy adsorption geometries for the PS were evaluated by examining several initial adsorption geometries on the MOF. For the lithium-containing molecules (Li_2S_4 and Li_2S), electrostatic considerations suggest that nominally positive lithium in the PS will be attracted to nominally negative oxygen atoms within the MOF. Likewise, electrostatic considerations suggest that nominally negative sulfur will be attracted to the CUS, which exhibits a nominal positive charge (formal charge of +2). The PS+M_2(dobdc) geometries were relaxed to a force tolerance of 0.02 eV/Å, while maintaining the full periodicity of the MOF crystal structure (i.e., cluster approximations to the MOF structure were not employed).

Adsorption energies (ΔE_{ads}) were evaluated using the following equation:

$$\Delta E_{ads} = -\frac{1}{n}(E_{MOF+PS} - E_{MOF} - nE_{PS})$$

We adopt a sign convention such that a positive ΔE_{ads} indicates exothermic adsorption. Here, n is the number of adsorbed polysulfide (PS) molecules in the M_2(dobdc) computational cell. E_{MOF+PS} refers to the total energies of the adsorbed MOF+PS complex. E_{MOF} and E_{PS} refer the total energies of isolated MOF and PS, respectively. The primitive cell for M_2(dobdc) was adopted as the simulation cell; this cell contains 54 atoms. A Bader charge analysis[67,68] was used to correlate adsorption energies with the amount of charge transfer between the adsorbed PS and the MOF support.

RESULTS AND DISCUSSION

Structure. Figure 1 shows the relaxed structures and bond lengths/angles of the isolated S_8, Li_2S_4, and Li_2S molecules.

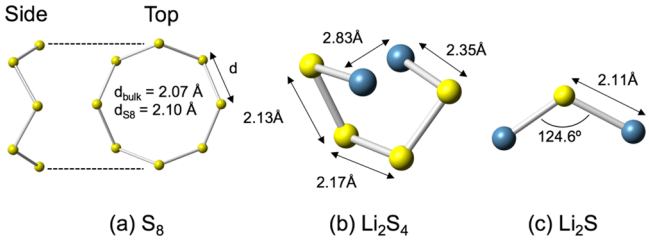

Figure 1. Calculated geometries for the molecular species (S_8, Li_2S_4, and Li_2S) examined in this study. Blue and yellow spheres represent lithium and sulfur, respectively.

These structures employed initial molecular geometries reported in an earlier study;[31] upon relaxation, they maintain a high degree of similarity. The S_8 molecule adopts a cyclo-octa ring morphology, similar to that present in the bulk sulfur crystal structure.[69] In the case of Li_2S_4, the lowest-energy structure exhibits a chainlike geometry with Li atoms located at both end points. Finally, Li_2S adopts a triangular geometry with a Li−S−Li angle of 124.6°.

The molecules' geometries upon adsorption in Ni_2(dobdc) are shown in Figure 2. In all cases, the lowest-energy adsorbed configurations place the molecules adjacent to the CUS. Moreover, sulfur atoms in the adsorbate are generally positioned to be closest to the CUS. In the case of S_8 (Figure 2a), the 8-membered ring is adsorbed with an orientation such that the plane of the ring is parallel to the axis of the hexagonal pore channel.

In the case of Li_2S_4, the calculations reveal that the molecule either can adsorb intact (Figure 2b) or, for certain CUS compositions, can spontaneously decompose (Figure 2c) into a Li_2S_2 molecule and a S_2 molecule. In this latter case, the Li_2S_2 and S_2 fragments adsorb on neighboring CUS. The intact cases comprise the majority of the adsorbed geometries observed, corresponding to 11 of the 16 examined CUS compositions. As shown in Figure 2b (bottom), these geometries generally exhibit close contact between a sulfur atom in the Li_2S_4 chain with the CUS. Additionally, the terminal lithium atoms in the adsorbate tend to be positioned adjacent to oxygen anions that are nearest-neighbors to the CUS. These geometries are consistent with the expected electrostatic interactions described previously.

Li_2S_4 was observed to undergo dissociative adsorption (Figure 2c) on the CUS for cases where M is an early transition metal, M = Sc, Ti, V, Cr, and Mo. As discussed below, Li_2S_4 dissociation correlates with very exothermic adsorption energies. Representative adsorbed geometries and summaries of calculated bond lengths for Li_2S_4 adsorption are given in Figure S1 and Table S1, respectively, for the dissociated case, and in Figure S2 and Table S2 for the intact case.

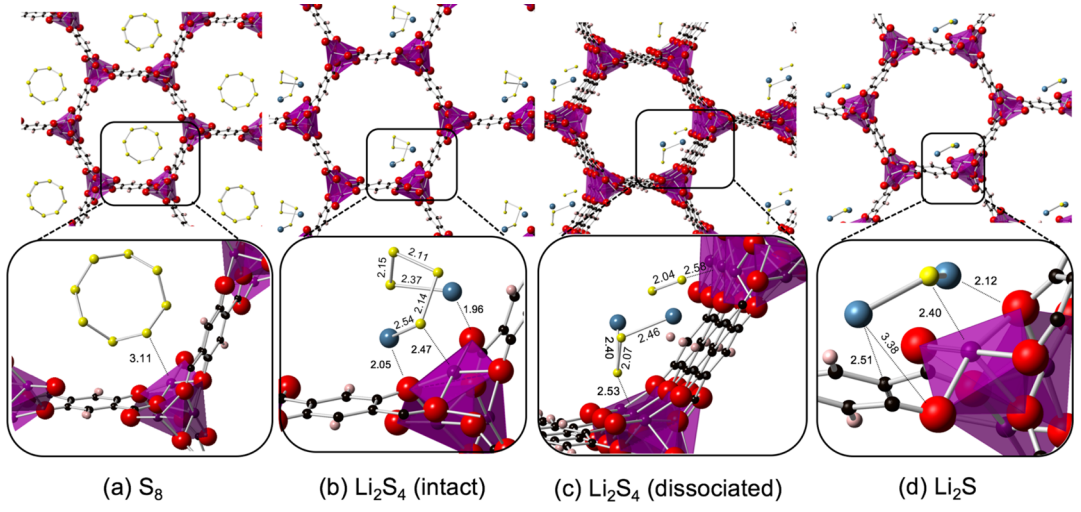

Figure 2. Lowest-energy structures for adsorbed (a) S_8, (b) intact and (c) dissociated Li_2S_4, and (d) Li_2S in Ni_2(dobdc). The top row shows the hexagonal pore structure of the MOF and the geometry of a single adsorbed molecule. The bottom row is a magnification of the region near the CUS, with selected bond lengths identified. Purple, red, and black spheres represent nickel, oxygen, and carbon atoms, respectively, in the MOF; blue and yellow represent Li and S in the adsorbate.

DOI: 10.1021/acs.chemmater.7b01166
Chem. Mater. XXXX, XXX, XXX−XXX

Unlike the behavior of Li_2S_4, the adsorption of Li_2S occurs with an intact geometry (Figure 2d), which is similar to that of the isolated molecule. Consistent with an electrostatic interaction, the S atom in Li_2S is in close proximity to the CUS, while at least one of the two Li atoms is adjacent to an O anion in the MOF. A list of bond lengths and angles for Li_2S upon adsorption to various M_2(dobdc) variants is given in Table S3. In general, the average distance between the CUS and the nearest S atom in the adsorbate is inversely correlated with the strength of adsorption (described below). These distances are 3.23 Å for S_8, 2.47 and 2.81 Å, respectively, for dissociated and intact Li_2S_4, and 2.58 Å for Li_2S. An illustration of the structure of adsorbed Li_2S in the vicinity of the CUS in Ni_2(dobdc) is given in Figure S3.

Energetics. The calculated adsorption energies for S_8, Li_2S_4, and Li_2S in M_2(dobdc) are plotted in Figure 3 as a function of the CUS composition. For Li_2S_4, separate adsorption energies were evaluated for intact and dissociated geometries. [For compositions where Li_2S_4 did not spontaneously dissociate, ΔE_{ads} for a (hypothetical) dissociated adsorbate was evaluated by initiating the relaxation from a dissociated geometry similar to that observed for the spontaneous cases.]

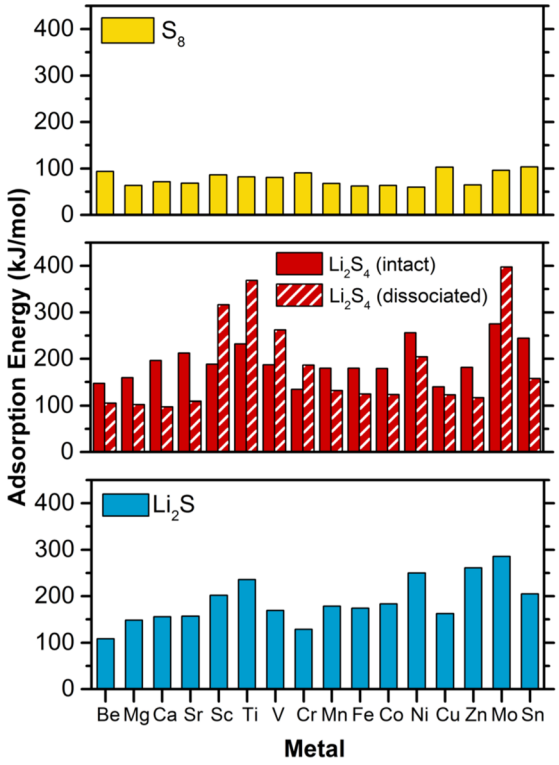

Figure 3. Calculated adsorption energies for S_8 (top), Li_2S_4 (middle, differentiating between intact and dissociated geometries), and Li_2S (bottom), as a function of CUS composition, M, within the MOF M_2(dobdc).

Averaging across the 16 CUS compositions, adsorption of S_8 is the weakest among all Li−S adsorbates examined, at 78 kJ/mol. At the opposite extreme, spontaneously dissociated Li_2S_4 exhibits the most exothermic adsorption energies, 306 kJ/mol on average. Finally, Li_2S and intact Li_2S_4 have intermediate values of 189 and 188 kJ/mol, respectively. To place these values in context, we note that adsorption energies for Li_2S_4 and Li_2S are (significantly) more exothermic than those reported previously for other small molecules such as CO_2, CH_4, and SO_2 within M_2(dobdc): for CH_4 and CO_2, ΔE_{ads} values less than 55 kJ/mol were reported.[40,70] The calculated ΔE_{ads} of 150 kJ/mol[66] for SO_2, which is a much more reactive species, also falls below the average values reported here for Li_2S_4 and Li_2S adsorption.

Turning first to the adsorption of S_8, Figure 3 (top) shows that the adsorption energy is relatively insensitive to the CUS composition, with ΔE_{ads} exhibiting a standard deviation of only 15 kJ/mol across the different metal compositions. The magnitude of the adsorption energies and limited sensitivity to the metal composition are consistent with a van der Waals interaction between the adsorbate and the MOF, augmented by a slight polarization of the S_8 (see the discussion of Electronic Structure below). A similar conclusion regarding the van der Waals nature of the adsorption interaction has been discussed in earlier reports.[34,69] For example, Cui et al. demonstrated that the adsorption energy for S_8 on various metal chalcogenides is relatively insensitive to composition—ranging from 72 to 82 kJ/mol—in very good agreement with the adsorption energies reported here.[34]

Adsorption energies for the polysulfides are generally more exothermic. In the case of Li_2S_4, Figure 3 (middle) summarizes ΔE_{ads} for both intact and dissociative adsorption. As previously described, dissociative adsorption is preferred for the early transition metals, M = Sc, Ti, V, Cr, and Mo, whereas intact adsorption prevails when the CUS composition is an alkaline earth metal or a mid- to late-series transition metal. Dissociative adsorption correlates strongly with highly exothermic adsorption: of the five MOF compositions with the largest ΔE_{ads}, four involve Li_2S_4 dissociation. The high intact ΔE_{ads} predicted on Ni_2(dobdc) represents the lone exception to this trend. The largest adsorption energy overall occurs for M = Ti and Mo, with values of 369 and 398 kJ/mol. These values exceed those for Li_2S_4 adsorption on metal chalcogenides, which achieved a maximum of 360 kJ/mol on V_2O_5,[34] suggesting an even greater tendency to suppress PS dissolution in these MOFs. (Although not discussed in detail here, Figure S4 compares the adsorption energies of S_2 in M_2(dobdc) to that of dissociated Li_2S_4. The adsorption trend across the various metal substitutions is observed to be similar for both molecules; this is expected given that S_2 are components of dissociated Li_2S_4.)

In the case of Li_2S, intact adsorption dominates. The predicted ΔE_{ads} values—while not as uniform with respect to CUS composition as for S_8—exhibit less variation than for Li_2S_4 adsorption. Nevertheless, some similarities with Li_2S_4 adsorption persist: for example, 4 of the top 5 most strongly adsorbing MOF compositions are the same for Li_2S and Li_2S_4. These include Sc, Ti, Ni, and Mo. Nevertheless, even in these exceptional cases, the magnitude of ΔE_{ads} for Li_2S is significantly smaller than that for Li_2S_4. For example, the maximum ΔE_{ads} for Li_2S is 286 kJ/mol in the case of Mo_2(dobdc); this is 112 kJ/mol smaller than that for Li_2S_4 adsorption on the same MOF.

Our observation that the adsorption of Li_2S in M_2(dobdc) is generally less exothermic than that for Li_2S_4 differs from the trend reported for the adsorption on metal chalcogenides,[34] where Li_2S adsorption was reported to be stronger. This difference can be traced to the highly exothermic nature of dissociative adsorption of Li_2S_4 in the MOF. In M_2(dobdc), dissociation can strengthen the attraction of Li_2S_4 to the MOF by more than 100 kJ/mol compared to the intact case. This is approximately twice the energy increment reported for dissociative adsorption on the metal chalcogenides.[34]

DOI: 10.1021/acs.chemmater.7b01166
Chem. Mater. XXXX, XXX, XXX−XXX

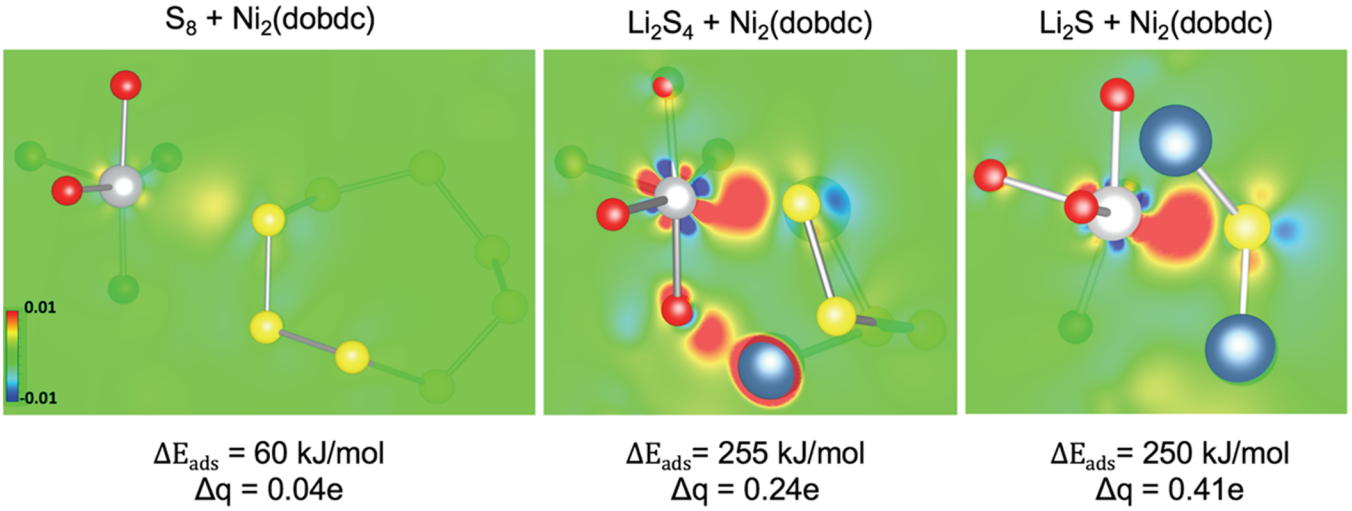

Figure 4. Charge density difference, $\rho_{adsorbed} - \sum\rho_{isolated}$, for S_8 (left), Li_2S_4 (middle), and Li_2S (right) adsorbed on Ni_2(dobdc). The plot is constructed for a plane that intersects the CUS−S bond axis and one other bonded pair of atoms in the adsorbate. For clarity, only the Ni CUS and its nearest-neighbor oxygens in the MOF are shown. Oxygen atoms are red, Ni is gray, sulfur is yellow, and Li is blue. Red shading corresponds to charge accumulation upon adsorption (maximum charge density = 0.01 e/bohr^3), and blue areas represent charge depletion (minimum density = −0.01 e/bohr^3). The corresponding adsorption energies and the amount of transferred charge from the molecule to M_2(dobdc) (from a Bader charge analysis) are summarized below each panel.

As described in the Introduction, by synthesizing variants of M_2(dobdc) with different CUS metals, it may be possible to tune the adsorption behavior of the PS and the redox end members (REM), S and Li_2S. The adsorption energies evaluated here allow us to identify potentially optimal M_2(dobdc) compositions. Our assessment is based on two assumptions: (*i*) stronger adsorption is preferred, as it will maximize the anchoring effect, and (*ii*) anchoring the PS is of greater importance than anchoring the REM, as the PS are more soluble, and thus more likely to "escape" from the cathode.

These factors suggest that optimal M_2(dobdc) compositions will be those having the largest adsorption energies for Li_2S_4. As shown in Figure 3, these compositions include M = Sc, Ti, V, Ni, and Mo. As an added benefit, 4 of these metals (Sc, Ti, Ni, and Mo) are within the top-5 compositions for adsorption of Li_2S (Figure 3), suggesting that strong anchoring of Li_2S should also be provided by these MOFs. The relatively weaker interaction between S_8 and all CUS compositions considered here suggests that S_8 adsorption is not a differentiating factor in identifying optimal M_2(dobdc) compositions.

Which of these compositions is most promising? Cost considerations suggest that scandium is impractical. Ease of synthesis is also an important consideration; to our knowledge, M_2(dobdc) variants with M = Ti, V, and Mo have not been reported. Finally, as a member of the 4d series, Mo is the heaviest candidate on our list; this could compromise the cell's specific energy.

Thus, the process of elimination leads us to Ni_2(dobdc) as the most promising Li−S cathode support. We note that Ni_2(dobdc) has been successfully sunthesized.[71] The unique ability of this MOF to bind Li_2S_4 strongly with an intact morphology (Figure 3) may also yield kinetic benefits compared to metals that dissociate the PS. Our prediction that Ni_2(dobdc) is the most promising composition in the M_2(dobdc) series is consistent with the experimental measurements of Zheng et al., who reported that a MOF with a Ni-based CUS outperformed the analogous Co-CUS compound in a Li−S cell.[54]

Because many MOFs are electrical insulators, conduction-enhancing additives such as carbon may be needed in MOF-based cathodes to ensure sufficient electronic transport. Recent work, however, has shown the possibility of overcoming this limitation, with conductivities of mS/cm or higher having been reported in selected MOFs.[72] Notably, a conductivity of 7 S/m was reported in HKUST-1, a CUS-containing MOF that has been infiltrated with redox-active guest molecules.[73]

Electronic Structure. Figure 4 compares charge density differences, adsorption energies, and the amount of charge transferred (from adsorbate to MOF) for S_8, Li_2S_4, and Li_2S adsorption on Ni_2(dobdc). As expected, the degree of charge transfer generally increases from S_8 to either Li_2S_4 or Li_2S, roughly consistent with the adsorption energies. A similar trend is observed for the charge density difference maps, which indicate larger charge accumulation between the CUS cations and S atoms in Li_2S_4 and Li_2S compared to that for S_8 adsorption. Additional charge accumulation is observed between the Li ions in Li_2S_4 and Li_2S and the O atoms in the MOF nearest to the CUS (Figure S5).

Table S4 summarizes the degree of charge transfer—evaluated as the difference in summed Bader charges, before and after adsorption—associated with adsorption across the various M_2(dobdc) compositions and adsorbates. Here, positive values refer to charge accumulation on the MOF, and *vice versa*. For the adsorption of S_8, the amount of charge transferred is negligible across the M_2(dobdc) variants, 0.04 e, on average, lending additional support to the assertion that S_8 adsorption can be described by a relatively weak van der Waals interaction.[74]

Electrostatic interactions contribute to the larger adsorption energies observed for Li_2S_4 and Li_2S. Turning first to Li_2S_4, Table S4 demonstrates that the amount of charge transferred on average between Li_2S_4 and the MOF is 4 (intact adsorption) to 7 (dissociative adsorption) times larger than that for S_8 adsorption, consistent with the trend in adsorption energies.

DOI: 10.1021/acs.chemmater.7b01166
Chem. Mater. XXXX, XXX, XXX−XXX

For intact Li_2S_4 adsorption, a relatively small amount of charge is transferred to the MOF for all metal compositions, approximately 0.25 e or less. In contrast, for dissociative Li_2S_4 adsorption involving M = Sc, Ti, V, Cr, and Mo, the charge transfer direction is reversed, with a net charge accumulation on the Li_2S_4 fragments. In these cases, the magnitude of charge transfer is also much larger, ranging from about 0.5 to 1.2 electrons.

Finally, Li_2S adsorption exhibits the largest average charge transfer with the MOF, 0.39 e. The net transfer is to the MOF for all metal compositions, and the average amount of charge transferred is approximately twice that for intact Li_2S_4 adsorption. We note that the charge transfer trends between Li_2S and intact Li_2S_4 adsorption are not reflected in their average ΔE_{ads} values, which are nearly identical (~190 kJ/mol). This apparent discrepancy can be explained by size differences between these molecules: smaller Li_2S has fewer, but stronger, interactions with the MOF, whereas the larger size of Li_2S_4 allows for more numerous bonding interactions that are relatively weaker, on average.

CONCLUSION

A means to suppress the dissolution of polysulfides will accelerate the commercialization of Li−S batteries. Toward this goal, the present study has explored the use of MOFs as PS-constraining cathode support materials. MOFs are promising support materials because the intrinsic encapsulation afforded by MOF pores can be augmented by chemical adsorption of PS onto coordinately unsaturated metal sites (CUS).

We demonstrate that the combination of PS encapsulation and adsorption can be tuned to maximize PS anchoring via substitution on the CUS. Optimal compositions are pinpointed by computationally screening 16 metal-substituted variants of M_2(dobdc) (MOF-74) for their ability to chemically anchor prototypical species (S_8, Li_2S_4, and Li_2S) present during the cycling of Li−S batteries. Importantly, the adsorption capacity of M_2(dobdc) is predicted to range from 6.6 to 13.4 mg of Li_2S_4 per 10 mg of MOF. These theoretical capacities outperform the best sulfur support material demonstrated in the literature, MnO_2, which has a capacity of ~6 mg of Li_2S_4/10 mg of MnO_2.

Our calculations reveal that the CUS is the dominant adsorption site for all species examined. Nevertheless, significant differences exist in the strength and nature of the adsorption across the three adsorbates. Adsorption of S_8 was observed to be relatively weak and insensitive to the composition of the CUS, consistent with a van der Waals-type interaction. In contrast, adsorption of Li_2S_4 and Li_2S is predicted to be much stronger, approaching ~400 kJ/mol, and is highly sensitive to CUS composition. A tendency for spontaneous decomposition of the Li_2S_4 molecule was observed on Sc_2, Ti_2, V_2, and Mo_2(dobdc), yielding very strong adsorption. The calculated adsorption energies can exceed those reported for Li_2S_4 adsorption on metal chalcogenides, suggesting an even greater tendency to suppress PS dissolution in M_2(dobdc). Analysis of Bader charges and charge density difference maps reveals that electrostatic interactions contribute to the large adsorption energies observed for Li_2S_4 and Li_2S.

Finally, Ti_2, Ni_2, and Mo_2(dobdc) were identified as the compositions with the largest affinities for Li_2S_4 and Li_2S. As Ni_2(dobdc) has been synthesized previously, this MOF is proposed as a promising cathode support for Li−S batteries.

ASSOCIATED CONTENT

Supporting Information

The Supporting Information is available free of charge on the ACS Publications website at DOI: 10.1021/acs.chemmater.7b01166.

The structure of S_8, Li_2S, and Li_2S_4 adsorbed on Ni_2(dobdc); calculated distances between adsorbate atoms and M_2(dobdc); adsorption energies for S_2 and dissociated Li_2S_4 on M_2(dobdc); charge density difference plots between O atoms in Ni_2(dobdc) and Li atoms in adsorbed molecules; the amount of charge transfer associated with adsorption on M_2(dobdc) across the different adsorbates (PDF)

AUTHOR INFORMATION

Corresponding Author

*E-mail: djsiege@umich.edu.. Tel.: +1 (734) 764-4808.

ORCID

Haesun Park: 0000-0001-6266-8151

Donald J. Siegel: 0000-0001-7913-2513

Notes

The authors declare no competing financial interest.

ACKNOWLEDGMENTS

This work was supported as part of the Joint Center for Energy Storage Research (JCESR), an Energy Innovation Hub funded by the U.S. Department of Energy, Office of Science, and Basic Energy Sciences.

REFERENCES

(1) Bruce, P. G.; Freunberger, S. A.; Hardwick, L. J.; Tarascon, J.-M. Li−O_2 and Li−S batteries with high energy storage. *Nat. Mater.* **2012**, *11*, 172.

(2) Cairns, E. J.; Albertus, P. Batteries for Electric and Hybrid-Electric Vehicles. *Annu. Rev. Chem. Biomol. Eng.* **2010**, *1*, 299−320.

(3) Manthiram, A.; Chung, S.-H.; Zu, C. Lithium−Sulfur Batteries: Progress and Prospects. *Adv. Mater.* **2015**, *27*, 1980−2006.

(4) Mikhaylik, Y. V.; Akridge, J. R. Polysulfide Shuttle Study in the Li/S Battery System. *J. Electrochem. Soc.* **2004**, *151*, A1969−A1976.

(5) Xiao, L.; Cao, Y.; Xiao, J.; Schwenzer, B.; Engelhard, M. H.; Saraf, L. V.; Nie, Z.; Exarhos, G. J.; Liu, J. A Soft Approach to Encapsulate Sulfur: Polyaniline Nanotubes for Lithium-Sulfur Batteries with Long Cycle Life. *Adv. Mater.* **2012**, *24*, 1176−1181.

(6) Zheng, J.; Lv, D.; Gu, M.; Wang, C.; Zhang, J.-G.; Liu, J.; Xiao, J. How to Obtain Reproducible Results for Lithium Sulfur Batteries? *J. Electrochem. Soc.* **2013**, *160*, A2288−A2292.

(7) Wang, L.; Liu, J.; Yuan, S.; Wang, Y.; Xia, Y. To mitigate self-discharge of lithium-sulfur batteries by optimizing ionic liquid electrolytes. *Energy Environ. Sci.* **2016**, *9*, 224−231.

(8) Zhou, W.; Wang, C.; Zhang, Q.; Abruña, H. D.; He, Y.; Wang, J.; Mao, S. X.; Xiao, X. Tailoring Pore Size of Nitrogen-Doped Hollow Carbon Nanospheres for Confining Sulfur in Lithium−Sulfur Batteries. *Adv. Energy Mater.* **2015**, *5*, 1401752.

(9) Zhou, G.; Zhao, Y.; Manthiram, A. Dual-Confined Flexible Sulfur Cathodes Encapsulated in Nitrogen-Doped Double-Shelled Hollow Carbon Spheres and Wrapped with Graphene for Li−S Batteries. *Adv. Energy Mater.* **2015**, *5*, 1402263.

(10) Zhou, G.; Paek, E.; Hwang, G. S.; Manthiram, A. Long-life Li/polysulphide batteries with high sulphur loading enabled by light-weight three-dimensional nitrogen/sulphur-codoped graphene sponge. *Nat. Commun.* **2015**, *6*, 7760.

(11) Zhang, S. S. Heteroatom-doped carbons: synthesis, chemistry and application in lithium/sulphur batteries. *Inorg. Chem. Front.* **2015**, *2*, 1059−1069.

DOI: 10.1021/acs.chemmater.7b01166
Chem. Mater. XXXX, XXX, XXX−XXX

(12) Song, J.; Gordin, M. L.; Xu, T.; Chen, S.; Yu, Z.; Sohn, H.; Lu, J.; Ren, Y.; Duan, Y.; Wang, D. Strong Lithium Polysulfide Chemisorption on Electroactive Sites of Nitrogen-Doped Carbon Composites For High-Performance Lithium−Sulfur Battery Cathodes. *Angew. Chem., Int. Ed.* **2015**, *54*, 4325−4329.
(13) Pang, Q.; Tang, J.; Huang, H.; Liang, X.; Hart, C.; Tam, K. C.; Nazar, L. F. A Nitrogen and Sulfur Dual-Doped Carbon Derived from Polyrhodanine@Cellulose for Advanced Lithium−Sulfur Batteries. *Adv. Mater.* **2015**, *27*, 6021−6028.
(14) Song, J.; Xu, T.; Gordin, M. L.; Zhu, P.; Lv, D.; Jiang, Y.-B.; Chen, Y.; Duan, Y.; Wang, D. Nitrogen-Doped Mesoporous Carbon Promoted Chemical Adsorption of Sulfur and Fabrication of High-Areal-Capacity Sulfur Cathode with Exceptional Cycling Stability for Lithium-Sulfur Batteries. *Adv. Funct. Mater.* **2014**, *24*, 1243−1250.
(15) Rong, J.; Ge, M.; Fang, X.; Zhou, C. Solution Ionic Strength Engineering As a Generic Strategy to Coat Graphene Oxide (GO) on Various Functional Particles and Its Application in High-Performance Lithium−Sulfur (Li−S) Batteries. *Nano Lett.* **2014**, *14*, 473−479.
(16) Qiu, Y.; Li, W.; Zhao, W.; Li, G.; Hou, Y.; Liu, M.; Zhou, L.; Ye, F.; Li, H.; Wei, Z.; Yang, S.; Duan, W.; Ye, Y.; Guo, J.; Zhang, Y. High-Rate, Ultralong Cycle-Life Lithium/Sulfur Batteries Enabled by Nitrogen-Doped Graphene. *Nano Lett.* **2014**, *14*, 4821−4827.
(17) He, G.; Hart, C. J.; Liang, X.; Garsuch, A.; Nazar, L. F. Stable Cycling of a Scalable Graphene-Encapsulated Nanocomposite for Lithium−Sulfur Batteries. *ACS Appl. Mater. Interfaces* **2014**, *6*, 10917−10923.
(18) Song, M.-K.; Zhang, Y.; Cairns, E. J. A Long-Life, High-Rate Lithium/Sulfur Cell: A Multifaceted Approach to Enhancing Cell Performance. *Nano Lett.* **2013**, *13*, 5891−5899.
(19) Zhang, L.; Ji, L.; Glans, P.-A.; Zhang, Y.; Zhu, J.; Guo, J. Electronic structure and chemical bonding of a graphene oxide-sulfur nanocomposite for use in superior performance lithium-sulfur cells. *Phys. Chem. Chem. Phys.* **2012**, *14*, 13670−13675.
(20) Wang, H.; Yang, Y.; Liang, Y.; Robinson, J. T.; Li, Y.; Jackson, A.; Cui, Y.; Dai, H. Graphene-Wrapped Sulfur Particles as a Rechargeable Lithium−Sulfur Battery Cathode Material with High Capacity and Cycling Stability. *Nano Lett.* **2011**, *11*, 2644−2647.
(21) Ji, L.; Rao, M.; Zheng, H.; Zhang, L.; Li, Y.; Duan, W.; Guo, J.; Cairns, E. J.; Zhang, Y. Graphene Oxide as a Sulfur Immobilizer in High Performance Lithium/Sulfur Cells. *J. Am. Chem. Soc.* **2011**, *133*, 18522−18525.
(22) Ji, X.; Lee, K. T.; Nazar, L. F. A highly ordered nanostructured carbon-sulphur cathode for lithium-sulphur batteries. *Nat. Mater.* **2009**, *8*, 500−506.
(23) Strubel, P.; Thieme, S.; Biemelt, T.; Helmer, A.; Oschatz, M.; Brückner, J.; Althues, H.; Kaskel, S. ZnO Hard Templating for Synthesis of Hierarchical Porous Carbons with Tailored Porosity and High Performance in Lithium-Sulfur Battery. *Adv. Funct. Mater.* **2015**, *25*, 287−297.
(24) Li, Z.; Jiang, Y.; Yuan, L.; Yi, Z.; Wu, C.; Liu, Y.; Strasser, P.; Huang, Y. A Highly Ordered Meso@Microporous Carbon-Supported Sulfur@Smaller Sulfur Core−Shell Structured Cathode for Li−S Batteries. *ACS Nano* **2014**, *8*, 9295−9303.
(25) He, G.; Evers, S.; Liang, X.; Cuisinier, M.; Garsuch, A.; Nazar, L. F. Tailoring Porosity in Carbon Nanospheres for Lithium−Sulfur Battery Cathodes. *ACS Nano* **2013**, *7*, 10920−10930.
(26) Xin, S.; Gu, L.; Zhao, N.-H.; Yin, Y.-X.; Zhou, L.-J.; Guo, Y.-G.; Wan, L.-J. Smaller Sulfur Molecules Promise Better Lithium−Sulfur Batteries. *J. Am. Chem. Soc.* **2012**, *134*, 18510−18513.
(27) Jayaprakash, N.; Shen, J.; Moganty, S. S.; Corona, A.; Archer, L. A. Porous Hollow Carbon@Sulfur Composites for High-Power Lithium−Sulfur Batteries. *Angew. Chem.* **2011**, *123*, 6026−6030.
(28) Pang, Q.; Liang, X.; Kwok, C. Y.; Nazar, L. F. Advances in lithium−sulfur batteries based on multifunctional cathodes and electrolytes. *Nat. Energy* **2016**, *1*, 16132.
(29) Hart, C. J.; Cuisinier, M.; Liang, X.; Kundu, D.; Garsuch, A.; Nazar, L. F. Rational design of sulphur host materials for Li-S batteries: correlating lithium polysulphide adsorptivity and self-discharge capacity loss. *Chem. Commun.* **2015**, *51*, 2308−2311.
(30) Ji, X.; Evers, S.; Black, R.; Nazar, L. F. Stabilizing lithium−sulphur cathodes using polysulphide reservoirs. *Nat. Commun.* **2011**, *2*, 325.
(31) Evers, S.; Yim, T.; Nazar, L. F. Understanding the Nature of Absorption/Adsorption in Nanoporous Polysulfide Sorbents for the Li−S Battery. *J. Phys. Chem. C* **2012**, *116*, 19653−19658.
(32) Seh, Z. W.; Li, W.; Cha, J. J.; Zheng, G.; Yang, Y.; McDowell, M. T.; Hsu, P.-C.; Cui, Y. Sulphur−TiO_2 yolk−shell nanoarchitecture with internal void space for long-cycle lithium−sulphur batteries. *Nat. Commun.* **2013**, *4*, 1331.
(33) Seh, Z. W.; Yu, J. H.; Li, W.; Hsu, P.-C.; Wang, H.; Sun, Y.; Yao, H.; Zhang, Q.; Cui, Y. Two-dimensional layered transition metal disulphides for effective encapsulation of high-capacity lithium sulphide cathodes. *Nat. Commun.* **2014**, *5*, 5017.
(34) Zhang, Q.; Wang, Y.; Seh, Z. W.; Fu, Z.; Zhang, R.; Cui, Y. Understanding the Anchoring Effect of Two-Dimensional Layered Materials for Lithium−Sulfur Batteries. *Nano Lett.* **2015**, *15*, 3780−3786.
(35) Kim, H.; Lee, J. T.; Lee, D.-C.; Magasinski, A.; Cho, W.-i.; Yushin, G. Plasma-Enhanced Atomic Layer Deposition of Ultrathin Oxide Coatings for Stabilized Lithium−Sulfur Batteries. *Adv. Energy Mater.* **2013**, *3*, 1308−1315.
(36) Tao, X.; Wang, J.; Ying, Z.; Cai, Q.; Zheng, G.; Gan, Y.; Huang, H.; Xia, Y.; Liang, C.; Zhang, W.; Cui, Y. Strong Sulfur Binding with Conducting Magnéli-Phase Ti_nO_{2n-1} Nanomaterials for Improving Lithium−Sulfur Batteries. *Nano Lett.* **2014**, *14*, 5288−5294.
(37) Yao, H.; Zheng, G.; Hsu, P.-C.; Kong, D.; Cha, J. J.; Li, W.; Seh, Z. W.; McDowell, M. T.; Yan, K.; Liang, Z.; Narasimhan, V. K.; Cui, Y. Improving lithium−sulphur batteries through spatial control of sulphur species deposition on a hybrid electrode surface. *Nat. Commun.* **2014**, *5*, 3943.
(38) Jiang, J.; Zhu, J.; Ai, W.; Wang, X.; Wang, Y.; Zou, C.; Huang, W.; Yu, T. Encapsulation of sulfur with thin-layered nickel-based hydroxides for long-cyclic lithium−sulfur cells. *Nat. Commun.* **2015**, *6*, 8622.
(39) Xiao, Z.; Yang, Z.; Wang, L.; Nie, H.; Zhong, M. e.; Lai, Q.; Xu, X.; Zhang, L.; Huang, S. A Lightweight TiO_2/Graphene Interlayer, Applied as a Highly Effective Polysulfide Absorbent for Fast, Long-Life Lithium−Sulfur Batteries. *Adv. Mater.* **2015**, *27*, 2891−2898.
(40) Koh, H. S.; Rana, M. K.; Hwang, J.; Siegel, D. J. Thermodynamic screening of metal-substituted MOFs for carbon capture. *Phys. Chem. Chem. Phys.* **2013**, *15*, 4573−4581.
(41) Bae, Y.-S.; Liu, J.; Wilmer, C. E.; Sun, H.; Dickey, A. N.; Kim, M. B.; Benin, A. I.; Willis, R. R.; Barpaga, D.; LeVan, M. D.; Snurr, R. Q. The effect of pyridine modification of Ni-DOBDC on CO_2 capture under humid conditions. *Chem. Commun.* **2014**, *50*, 3296−3298.
(42) Rana, M. K.; Koh, H. S.; Hwang, J.; Siegel, D. J. Comparing van der Waals Density Functionals for CO_2 Adsorption in Metal Organic Frameworks. *J. Phys. Chem. C* **2012**, *116*, 16957−16968.
(43) Peng, Y.; Krungleviciute, V.; Eryazici, I.; Hupp, J. T.; Farha, O. K.; Yildirim, T. Methane Storage in Metal−Organic Frameworks: Current Records, Surprise Findings, and Challenges. *J. Am. Chem. Soc.* **2013**, *135*, 11887−11894.
(44) Koh, H. S.; Rana, M. K.; Wong-Foy, A. G.; Siegel, D. J. Predicting Methane Storage in Open-Metal-Site Metal−Organic Frameworks. *J. Phys. Chem. C* **2015**, *119*, 13451−13458.
(45) Ming, Y.; Purewal, J.; Yang, J.; Xu, C.; Veenstra, M.; Gaab, M.; Müller, U.; Siegel, D. J. Stability of MOF-5 in a hydrogen gas environment containing fueling station impurities. *Int. J. Hydrogen Energy* **2016**, *41*, 9374−9382.
(46) Goldsmith, J.; Wong-Foy, A. G.; Cafarella, M. J.; Siegel, D. J. Theoretical Limits of Hydrogen Storage in Metal−Organic Frameworks: Opportunities and Trade-Offs. *Chem. Mater.* **2013**, *25*, 3373−3382.
(47) Purewal, J.; Liu, D.; Sudik, A.; Veenstra, M.; Yang, J.; Maurer, S.; Müller, U.; Siegel, D. J. Improved Hydrogen Storage and Thermal Conductivity in High-Density MOF-5 Composites. *J. Phys. Chem. C* **2012**, *116*, 20199−20212.

DOI: 10.1021/acs.chemmater.7b01166
Chem. Mater. XXXX, XXX, XXX−XXX

(48) Caskey, S. R.; Wong-Foy, A. G.; Matzger, A. J. Dramatic Tuning of Carbon Dioxide Uptake via Metal Substitution in a Coordination Polymer with Cylindrical Pores. *J. Am. Chem. Soc.* **2008**, *130*, 10870−10871.
(49) Kapelewski, M. T.; Geier, S. J.; Hudson, M. R.; Stück, D.; Mason, J. A.; Nelson, J. N.; Xiao, D. J.; Hulvey, Z.; Gilmour, E.; FitzGerald, S. A.; Head-Gordon, M.; Brown, C. M.; Long, J. R. M2(m-dobdc) (M = Mg, Mn, Fe, Co, Ni) Metal−Organic Frameworks Exhibiting Increased Charge Density and Enhanced H_2 Binding at the Open Metal Sites. *J. Am. Chem. Soc.* **2014**, *136*, 12119−12129.
(50) Demir-Cakan, R.; Morcrette, M.; Nouar, F.; Davoisne, C.; Devic, T.; Gonbeau, D.; Dominko, R.; Serre, C.; Férey, G.; Tarascon, J.-M. Cathode Composites for Li−S Batteries via the Use of Oxygenated Porous Architectures. *J. Am. Chem. Soc.* **2011**, *133*, 16154−16160.
(51) Zhou, J.; Li, R.; Fan, X.; Chen, Y.; Han, R.; Li, W.; Zheng, J.; Wang, B.; Li, X. Rational design of a metal-organic framework host for sulfur storage in fast, long-cycle Li-S batteries. *Energy Environ. Sci.* **2014**, *7*, 2715−2724.
(52) Wang, Z.; Li, X.; Cui, Y.; Yang, Y.; Pan, H.; Wang, Z.; Wu, C.; Chen, B.; Qian, G. A Metal−Organic Framework with Open Metal Sites for Enhanced Confinement of Sulfur and Lithium−Sulfur Battery of Long Cycling Life. *Cryst. Growth Des.* **2013**, *13*, 5116−5120.
(53) Wang, Z.; Wang, B.; Yang, Y.; Cui, Y.; Wang, Z.; Chen, B.; Qian, G. Mixed-Metal−Organic Framework with Effective Lewis Acidic Sites for Sulfur Confinement in High-Performance Lithium−Sulfur Batteries. *ACS Appl. Mater. Interfaces* **2015**, *7*, 20999−21004.
(54) Zheng, J.; Tian, J.; Wu, D.; Gu, M.; Xu, W.; Wang, C.; Gao, F.; Engelhard, M. H.; Zhang, J.-G.; Liu, J.; Xiao, J. Lewis Acid−Base Interactions between Polysulfides and Metal Organic Framework in Lithium Sulfur Batteries. *Nano Lett.* **2014**, *14*, 2345−2352.
(55) Wiers, B. M.; Foo, M.-L.; Balsara, N. P.; Long, J. R. A Solid Lithium Electrolyte via Addition of Lithium Isopropoxide to a Metal−Organic Framework with Open Metal Sites. *J. Am. Chem. Soc.* **2011**, *133*, 14522−14525.
(56) Bai, S.; Liu, X.; Zhu, K.; Wu, S.; Zhou, H. Metal−organic framework-based separator for lithium−sulfur batteries. *Nat. Energy* **2016**, *1*, 16094.
(57) Cuisinier, M.; Cabelguen, P. E.; Adams, B. D.; Garsuch, A.; Balasubramanian, M.; Nazar, L. F. Unique behaviour of nonsolvents for polysulphides in lithium-sulphur batteries. *Energy Environ. Sci.* **2014**, *7*, 2697−2705.
(58) Suo, L.; Hu, Y.-S.; Li, H.; Armand, M.; Chen, L. A new class of Solvent-in-Salt electrolyte for high-energy rechargeable metallic lithium batteries. *Nat. Commun.* **2013**, *4*, 1481.
(59) Dokko, K.; Tachikawa, N.; Yamauchi, K.; Tsuchiya, M.; Yamazaki, A.; Takashima, E.; Park, J.-W.; Ueno, K.; Seki, S.; Serizawa, N.; Watanabe, M. Solvate Ionic Liquid Electrolyte for Li−S Batteries. *J. Electrochem. Soc.* **2013**, *160*, A1304−A1310.
(60) Hohenberg, P.; Kohn, W. Inhomogeneous Electron Gas. *Phys. Rev.* **1964**, *136*, B864−B871.
(61) Blöchl, P. E. Projector augmented-wave method. *Phys. Rev. B: Condens. Matter Mater. Phys.* **1994**, *50*, 17953−17979.
(62) Kresse, G.; Furthmüller, J. Efficient iterative schemes for *ab initio* total-energy calculations using a plane-wave basis set. *Phys. Rev. B: Condens. Matter Mater. Phys.* **1996**, *54*, 11169−11186.
(63) Lee, K.; Murray, É. D.; Kong, L.; Lundqvist, B. I.; Langreth, D. C. Higher-accuracy van der Waals density functional. *Phys. Rev. B: Condens. Matter Mater. Phys.* **2010**, *82*, 081101.
(64) Dion, M.; Rydberg, H.; Schröder, E.; Langreth, D. C.; Lundqvist, B. I. Van der Waals Density Functional for General Geometries. *Phys. Rev. Lett.* **2004**, *92*, 246401.
(65) Dudarev, S. L.; Botton, G. A.; Savrasov, S. Y.; Humphreys, C. J.; Sutton, A. P. Electron-energy-loss spectra and the structural stability of nickel oxide: An LSDA+U study. *Phys. Rev. B: Condens. Matter Mater. Phys.* **1998**, *57*, 1505−1509.
(66) Lee, K.; Howe, J. D.; Lin, L.-C.; Smit, B.; Neaton, J. B. Small-Molecule Adsorption in Open-Site Metal−Organic Frameworks: A Systematic Density Functional Theory Study for Rational Design. *Chem. Mater.* **2015**, *27*, 668−678.
(67) Henkelman, G.; Arnaldsson, A.; Jónsson, H. A fast and robust algorithm for Bader decomposition of charge density. *Comput. Mater. Sci.* **2006**, *36*, 354−360.
(68) Tang, W.; Sanville, E.; Henkelman, G. A grid-based Bader analysis algorithm without lattice bias. *J. Phys.: Condens. Matter* **2009**, *21*, 084204.
(69) Park, H.; Koh, H. S.; Siegel, D. J. First-Principles Study of Redox End Members in Lithium−Sulfur Batteries. *J. Phys. Chem. C* **2015**, *119*, 4675−4683.
(70) Rana, M. K.; Koh, H. S.; Zuberi, H.; Siegel, D. J. Methane Storage in Metal-Substituted Metal−Organic Frameworks: Thermodynamics, Usable Capacity, and the Impact of Enhanced Binding Sites. *J. Phys. Chem. C* **2014**, *118*, 2929−2942.
(71) Dietzel, P. D. C.; Panella, B.; Hirscher, M.; Blom, R.; Fjellvag, H. Hydrogen adsorption in a nickel based coordination polymer with open metal sites in the cylindrical cavities of the desolvated framework. *Chem. Commun.* **2006**, 959−961.
(72) Sun, L.; Campbell, M. G.; Dincă, M. Electrically Conductive Porous Metal−Organic Frameworks. *Angew. Chem., Int. Ed.* **2016**, *55*, 3566−3579.
(73) Talin, A. A.; Centrone, A.; Ford, A. C.; Foster, M. E.; Stavila, V.; Haney, P.; Kinney, R. A.; Szalai, V.; El Gabaly, F.; Yoon, H. P.; Léonard, F.; Allendorf, M. D. Tunable Electrical Conductivity in Metal-Organic Framework Thin-Film Devices. *Science* **2014**, *343*, 66−69.
(74) Lee, L.-H. *Fundamentals of Adhesion*; Plenum Publishing Corporation: Webster, NY, 1991.

DOI: 10.1021/acs.chemmater.7b01166
Chem. Mater. XXXX, XXX, XXX−XXX